Effect of Contact Method between Interconnects and Electrodes on Area Specific Resistance in Planar Solid Oxide Fuel Cells

W. Wu[1], G. L. Wang[1], W. B. Guan[1]*, Y. F. Zhen[1], W. G. Wang[1]*

[1] Ningbo Institute of Material Technology and Engineering, Chinese Academy of Science 519 Zhuangshi Road, Zhenhai District, CN-315201, Ningbo, P. R. China

Abstract

In this work, interconnect/electrode sheet/interconnect sandwiches are assembled by designing interfacial contact between interconnects and electrodes for planar solid oxide fuel cells (SOFCs). Their area specific resistance (ASR) values of different contact methods under isothermal oxidation and thermal cycling are recorded by four-point method. The ASR of SUS430/Ni–YSZ/SUS430 anode sandwich with NiO current collecting layer is close to that of anode sandwich without NiO current collecting layer during isothermal operation, but smaller and more stable during thermal cycling. Meanwhile, the lowest ASR is obtained in SUS430/LSM–YSZ/SUS430 cathode sandwich with LSM coated interconnect and LSM current collecting layer among various contact methods between interconnects and cathodes,

and remains constant under isothermal oxidation and thermal cycling. Contact resistance between cathodes and interconnects is the main source of the SOFC stack resistance. A real stack with three anode-supported cells is assembled and tested under thermal cycling to verify the effect of different contact methods between interconnects and electrodes on performance of stack repeating unit. The degradation rate and ASR values of repeating unit inside the stack indicate that the contact between LSM coated interconnect and LSM current collecting layer on cathode side is the optimized contact.

Keywords: ASR, Contact, Solid Oxide Fuel Cell, Stack, Thermal Cycling

1 Introduction

A solid oxide fuel cell (SOFC) stack is generally composed of interconnects, sealing materials, and single cells [1]. With the decrease in operation temperature from 1,000 to below 850 °C, metallic materials have become the preferred choice for interconnects in SOFC stacks due to their advantages [2–4]. Among all metallic interconnects, Fe–Cr stainless steels, as the most favorable candidates, have been intensively investigated [5–9]. The area specific resistance (ASR) of Fe–Cr stainless steels in SOFC working temperature is around 0.01 Ω cm^2, which meets the requirement for interconnect application [10]. Moreover, improving the performance of single cells has also been widely conducted [11, 12]. However, neither the improvement of interconnects nor the progress in cell performance can yield the required level of improved stack output performance for SOFC commercialization. Researchers agree that the contact between metal interconnects

and cell electrodes is the most important factor for enhancing the stack output performance of planar SOFCs [13, 14].

Accordingly, optimizing the contact between interconnects and electrodes to reduce contact resistance has received increasing interests [15–17]. In 2003, Jiang et al. [15] found that the resistance composed of cell and contact resistance decreases from 1.43 to 0.19 Ω cm^2 at 800 °C when the contact area between the cathode and the current collecting layer increases from 4.6 to 27.2%. Meanwhile, Dey et al. [16], Bertrand et al. [17] and Magnière et al. [18] investigated the contact resistance between interconnects and electrodes quantitatively under different load, and found that the contact resistance can be reduced by the increasing compression loads. In this work, Ni–YSZ anode sheets, LSM–YSZ cathode sheets, and SUS430 metal interconnects were assembled into

a SUS430/electrode sheet/SUS430 sandwich to simulate different contact methods in accordance with the anode-supported Ni–YSZ/YSZ/LSM–YSZ stack structure design. The optimized contact was obtained by quantitatively evaluating the ASR between interconnects and electrodes by four-point method under the condition of isothermal oxidation as well as thermal cycling. Actual stack was also assembled and tested to verifying the sandwich results.

2 Experimental Procedures

Typical 10 cm × 10 cm Ni–YSZ anode sheets, composed of 44 wt.% YSZ and 56 wt.% NiO, and 10 cm × 10 cm LSM–YSZ cathode sheets, composed of 49 wt.% LSM and 51 wt.% YSZ, were manufactured by tape casting followed by sintering at 1,300 °C. The average thickness of the anode and cathode sheets after sintering was about 450 μm, which could ensure sufficient mechanical strength under compression load during testing. Commercial SUS430 metal was used as interconnects with an average thickness of 1.5 mm. The nominal composition of the commercial alloy was listed in Table 1. The gas channel and hexagonal contact tip of interconnect was obtained by etching method. The deep of gas channel and contact tip was about 0.6 mm and the length of the contact tip was also about 0.6 mm.

The $(La_{0.75}Sr_{0.25})_{0.95}MnO_{3-\sigma}$ (LSM) power prepared via Pechini route [19] was deposited on relevant interconnects as anti-oxidation coating by plasma spray with an average thickness of 30 μm. Before plasma spray, each interconnect substrate was ground to 600 grits with SiC sand paper, cleaned in acetone bath, and then sandblasted. The sandblasting treatment is one of the processes generally used to remove the impurity and oxide layer of interconnect substrate, and roughen the medium surface to obtain satisfactory adhesion of coatings [20]. Plasma spraying was conducted in Ar atmosphere with appropriate parameters listed in Table 2.

In the ASR test, the Ni–YSZ anode sheets, LSM–YSZ cathode sheets, and metallic interconnects were assembled into sandwich structures according to the configuration demonstrated in Figures 1 and 2, respectively. The active area of the anode and cathode sheets was 70 cm². The two-unit anode sandwich was composed of two anode sheets and three pieces of interconnects with nickel foam (purity: 99.9%, pore per inch: 110, density: 380 g m⁻², average pore size: 590 μm, thickness: 1.7 mm) from INCO (Dalian, China) Co. Ltd) on both sides. Anode sheet-1 was coated with a 20 μm layer of NiO by screen printing on each side, whereas anode sheet-2 had no NiO layer. As seen in Figure 1, anode unit 1 was composed of anode sheet-1 and interconnects, and anode unit 2 was composed of anode sheet-2 and interconnects.

Table 1 Chemical composition of SUS430 stainless steel.

Elements (wt.%)	Fe	Cr	Ni	C	Mn	Si	P
SUS430	Bal	16.14	0.044	–	0.209	0.279	0.028

Table 2 The plasma spray parameters.

Current (A)	Voltage (V)	Ar flow rate (L/H)	Powder feed rate (L/H)
600	55	1500	600

The three-unit cathode sandwich structure consisted of three LSM–YSZ cathode sheets and four pieces of metal interconnects. Cathode sheet-1 had no LSM cathode current collecting layer, whereas cathode sheet-2 and sheet-3 were coated with 250 μm LSM current collecting layer by screen printing on both sides. As seen in Figure 2, the repeating unit 1 was formed by cathode sheet-1 and uncoated interconnects, repeating unit 2 was composed of cathode sheet-2 and LSM-coated interconnects, and repeating unit 3 consisted of cathode sheet-3 and uncoated interconnects.

After assembly, the abovementioned sandwich structures were heated to 800 °C and kept for about 2 h in air under proper external load pressure. External load can result in lower contact resistance. Unit pressure of 700 g cm⁻² was adopted in this study according to Koch's work in 2004 [21]. The Ni–YSZ anode sandwich was tested in hydrogen atmosphere with a flow rate of 5 sccm cm⁻² (sccm is abbreviation of standard-state cubic centimeter per minute). And the LSM–YSZ cathode sandwich was tested in air atmosphere with a flow rate of 15 sccm cm⁻². The abovementioned sandwich structures were operated for about 200 h at 800 °C, and then subjected to thermal cycles from 800 °C to room temperature with a cooling and heating rate of 1 °C min⁻¹. During thermal cycling, a constant current of 0.1 A cm⁻² through the samples enabled a recording of the voltages. The ASR between cell electrodes and interconnects was calculated to observe the variation of voltages. The interfacial and cross-section microstructures of interconnects were analyzed by SEM (FEI Quanta FEG 250).

In investigating the performance of interconnects on the ASR of the sandwich structures, mass gain tests were carried
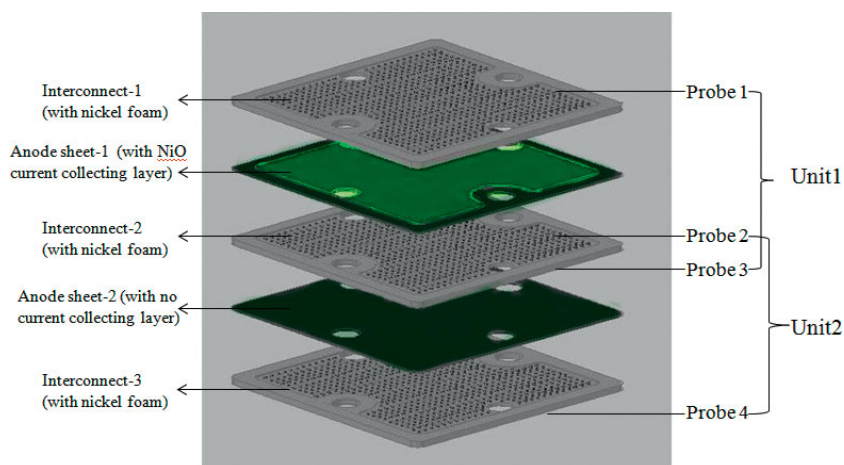

Fig. 1 SUS430/Ni–YSZ/SUS430 anode sandwich.

out. Accordingly, rectangular coupons with dimensions of 10×10 mm^2 were cut from interconnects and then hung in alumina crucibles in a furnace, which were oxidized at 800 °C in air for 200 h. The weight of each sample was measured immediately after cooling to room temperature.

To verifying the effect of contact method on the ASR between interconnects and electrodes, actual stack with three single cells was assembled and tested under thermal cycling from 800 to 100 °C. The single cell used in the stack was typical Ni–YSZ/YSZ/LSM anode-supported SOFCs with active area of 70 cm^2, which were manufactured by Ningbo Institute of Material Technology and Engineering, China. The manufacturing process and parameters of the cell were described in detail in the literature [22, 23]. The interfacial contact between interconnects and electrodes inside stack was designed in accordance with that of the sandwich experiment mentioned above. The stack configuration was demonstrated in Figure 3. Following assembly, the stack was placed in a furnace and heated to a certain temperature and then tested with pure H$_2$ as fuel and air as cathode gas. The process of heating and feeding gas can be seen in our previous published work [23]. During thermal cycling, each thermal cycle can be divided into two stages. The first stage involved cooling from 800 to 100 °C, followed by holding at 100 °C for about 2 h. The second stage involved heating from 100 to 800 °C, followed by holding at 800 °C for more than 6 h. A direct current (DC) of 0.1 A cm^{-2} was discharged. The length of each thermal cycle was 25 h.

3 Results and Discussions

The ASR of the sandwich structure can be calculated by the following equation:

$$\mathrm{ASR} = \frac{U \times S}{2I} \tag{1}$$

where I is the charging current, U is the output voltage, and S is the active area. Applying Eq. (1), Figure 4 presents the ASR results of the SUS430/Ni–YSZ/SUS430 anode sandwich structure. The ASR of anode unit 2 was 0.003 Ω cm^2 after 200 h of operation before thermal cycling, whereas that of anode unit 1 was about 0.004 Ω cm^2. The ASR of anode unit 1 and 2 was close approximately under isothermal operation.
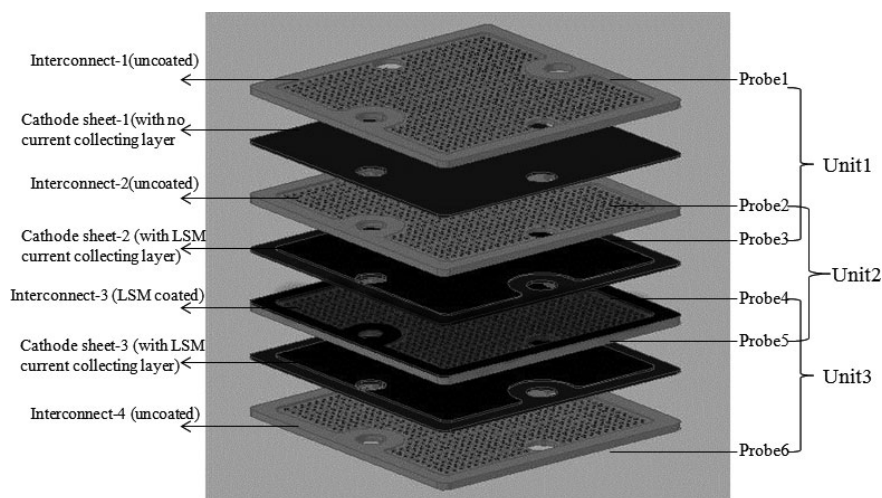
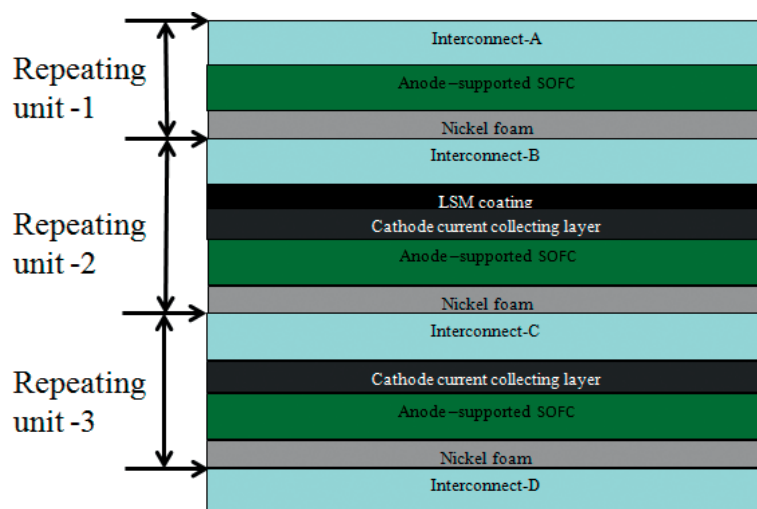

Fig. 2 SUS430/LSM–YSZ/SUS430 cathode sandwich.

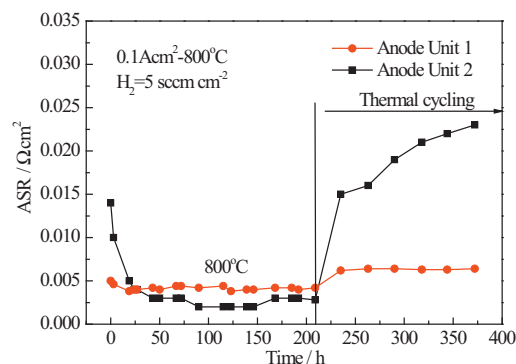Fig. 3 Schematic diagram of interface contact in stack research.

Fig. 4 The ASR of Anode sandwich *versus* running time and thermal cycles.

During thermal cycling, the ASR of anode unit 1 maintained 0.006 Ω cm^2 within six thermal cycles, showing excellent stability. However, the ASR of anode unit 2 increased rapidly from 0.003 to 0.015 Ω cm^2 after one thermal cycle and then

continued to increase with thermal cycles. After six thermal cycles, the ASR of anode unit 2 reached 0.023 Ω cm^2. According to our previous results [23], the ASR of one unit inside the stack was 0.6 Ω cm^2 owing to the proper sealing of the stack. Therefore, the measured maximum ASR value of the anode sandwich structures shared only 4% of that of one stack unit, indicating that the ASR of the anode side was considerably small for the total stack repeat unit resistance.

The ASR of the SUS430/LSM–YSZ/SUS430 cathode sandwich structure composed of LSM–YSZ cathode sheet and SUS430 metal interconnects can also be obtained by Eq. (1), as shown in Figure 5. During isothermal oxidation, the original ASR of cathode unit 2 (Figure 2) was 0.06 Ω cm^2, and then increased linearly with operation time to 0.11 Ω cm^2 after 200 h of isothermal oxidation. However, the ASR of cathode unit 1 and 3 increased follow parabolic law, increased from the original value of 0.9 and 0.07 Ω cm^2 to about 1.2 and 0.91 Ω cm^2, respectively. During thermal cycling, the ASR of cathode unit 2 increased to around 0.2 Ω cm^2 after one cycle and decreased linearly to 0.16 Ω cm^2 after six thermal cycles. The ASR value of cathode unit 3 was also increased after one cycle and decreased with time to about 1.04 Ω cm^2 after six thermal cycles. However, the ASR of cathode unit 1 increased dramatically to 3.8 Ω cm^2 after one thermal cycle and then still increased with thermal cycles. Finally, it reached 4.25 Ω cm^2 after six thermal cycles. It is obvious that the ASR of cathode unit 2 was the smallest among the three contact methods in this work during both isothermal oxidation and thermal cycles. Therefore, the measured maximum ASR value of the optimized cathode sandwich shared about 26.7% of that of one stack unit [23].

During thermal cycling, the LSM–YSZ cathode sandwich structure had a minimum ASR of 0.16 Ω cm^2 after the experiments. Meanwhile, the ASR of the Ni–YSZ anode sandwich structure had a minimum value of 0.006 Ω cm^2 and maximum value of 0.023 Ω cm^2. The minimum ASR of the cathode sandwich structure was about 7 and 27 times the maximum and minimum values of the anode sandwich structure, respectively. Meanwhile, the minimum ASR of the cathode
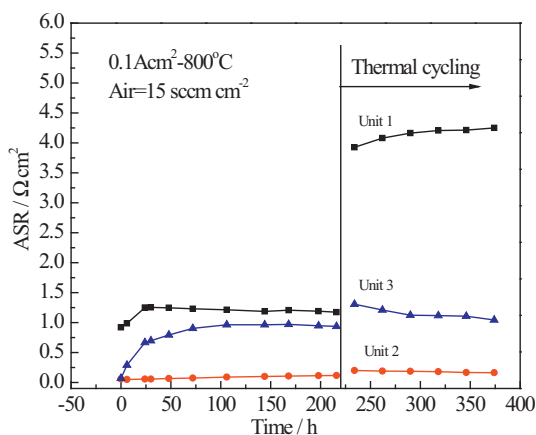
sandwich structure under isothermal oxidation was around 0.06 Ω cm^2, which was 15 times larger than the maximum value of anode side ASR (0.004 Ω cm^2) under the same condition. Therefore, contact resistance between SOFC cathodes and interconnects was dominant compared with that of the anode side.

The contact traces between sheets and interconnects were observed by optical microscope, as shown in Figure 6. No contact traces were found on the nickel foam surface left by the interconnect tips inside anode unit 1 after stable operation and six thermal cycles, whereas clear contact traces were left on the nickel foam by the interconnect tip inside anode unit 2. The absence of traces was attributable to the reduction of the NiO anode current collecting layer on anode sheet 1 to pure Ni. Moreover, pure Ni combined with the nickel foam on the anode sheet at high temperature by diffusion, resulting in unclear contact traces. In consequence, the presence of metallic contacts between interconnects and the current collecting layer produced a low interface resistance on the anode side [15]. For the anode without NiO coating, obvious traces were left by the direct hard contact between anode components, as shown in Figure 6b. During thermal cycling conditions, direct hard contact without NiO current collecting layer perhaps could be damaged by the CTE (co-efficient of thermal expansion) mismatch between interconnect and anode, resulting in the increase of ASR. The ASR results indicated that the NiO current collecting layer on the anode sheet can improve the contact between cell anodes and metal interconnects. However, the ASR values of the anode sandwich structure were considerably small whether with NiO current collecting layer or not.

The contact morphology of cathode sheets was also observed by optical microscope, as shown in Figure 7. Clear, regular, and deep traces were left on the cathode sheet-2 by the interconnect tip, and shallow traces were left on the cathode sheet-3 by the interconnect tip inside cathode unit 3. No traces could be found on the cathode sheet-1 inside cathode unit 1. According to the ASR results (Figure 5) and mass gain results (Figure 10), it can be seen that the ASR of cathode sandwich with uncoated interconnect and the mass gain of uncoated interconnect have the same increasing trends during the isothermal oxidation, indicating that the oxidation of interconnect is a crucial factor on the ASR of cathode side.
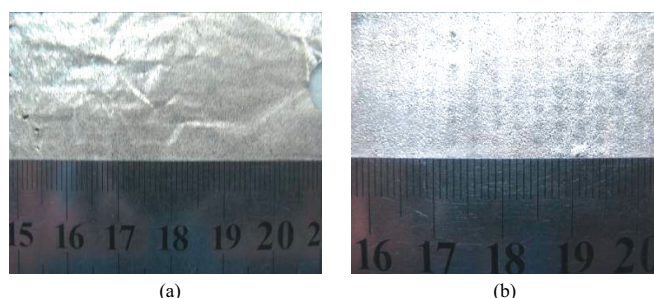

Fig. 5 The ASR of Cathode sandwich *versus* running time and thermal cycles.

Fig. 6 Contact traces on the foam nickel for (a) the anode with NiO current collecting layer; and (b) the anode without collecting layer.
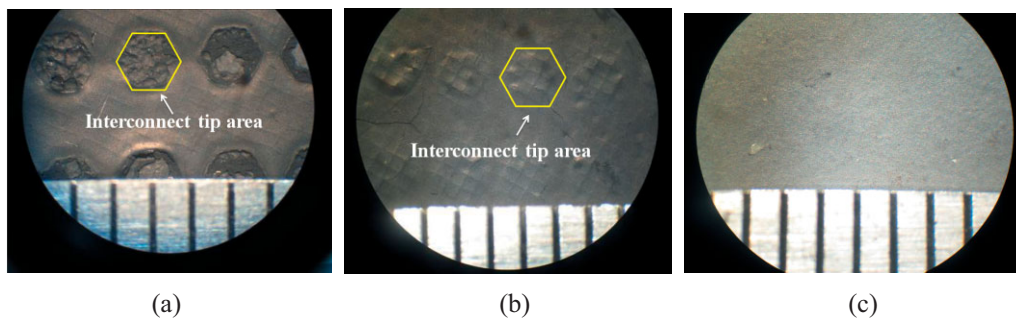
(a)   (b)   (c)

Fig. 7 Contact trace on cathode sheet left by interconnect for the sample with (a) coated interconnect and cathode current collecting layer, (b) coated interconnect and no cathode current collecting layer, and (c) uncoated interconnect and no cathode current collecting layer.
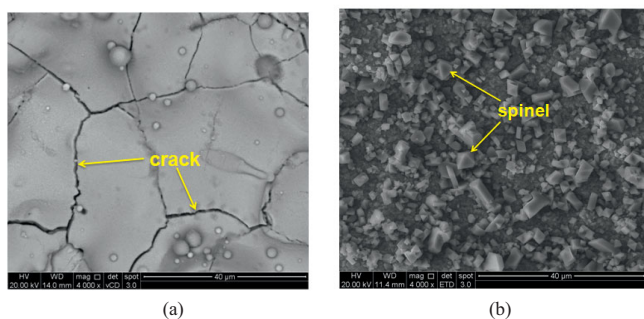

(a)   (b)

Fig. 8 SEM surface images of (a) LSM coated SUS430 stainless steel and (b) uncoated SUS430 stainless steel after operation at 800 °C for 200 h.
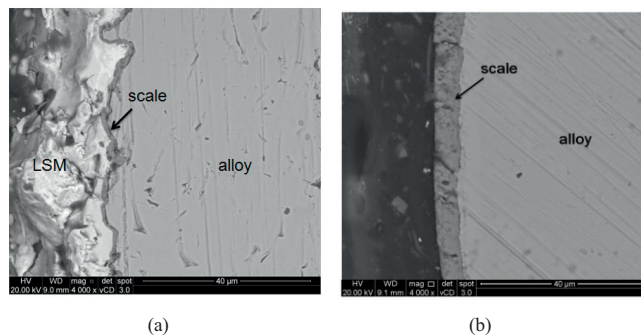

(a)   (b)

Fig. 9 SEM cross-section images of (a) LSM coated SUS430 stainless steel and (b) uncoated SUS430 stainless steel after operation at 800 °C for 200 h.

Figure 8a shows the surface morphology of the interconnect coated with LSM by plasma spray method, whereas Figure 8b presents the surface morphology of the uncoated interconnect after experiments. Numerous irregular-shaped grains formed on the bare steel after oxidation. LSM coating on the surface of the interconnect was uniform. However, some macro-cracks were found on the surface of LSM coating, which were caused by thin film shrinkage during the thermal cycling process. Figure 9 demonstrates the cross-section of coated and uncoated SUS430 stainless steel samples after the oxidation test at 800 °C. The outermost layer of the coated interconnect was dense LSM film. Under this layer was oxide scale of 2.5 μm in thickness. For the bare steel, the thickness of the scale that formed on the surface was about 8 μm. Evidently, the scale formed on the coated steel was much thinner than that of the bare steel due to positive effect of protective LSM coating. Figure 10 demonstrates the mass gain of the bare steel and LSM coated steel. It can be seen that the mass gain of the bare steel and LSM coated steel increased rapidly within 72 hours' isothermal oxidation. After that, the mass gain of the bare steel continued to increase slowly with time, while the mass gain of the LSM coated steel kept stable. Also, it can be seen that the mass gain of the coated steel was lower than that of the bare steel during the whole isothermal oxidation. The mass gain of the LSM-coated interconnect decreased by 56% when held at 800 °C for 200 h compared with that of bare steel, as shown in Figure 10. Generally, the electrical conductivity of the metallic interconnect depends more heavily on the electrical conductivity of the oxide scale
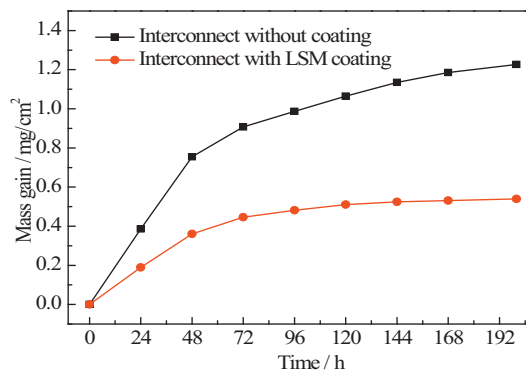

Fig. 10 Mass change of SUS430 stainless steel with and without LSM coating at 800 °C.

that formed on the surface after oxidation than on the metal itself [3]. As shown in Figure 9a, the scale thickness of LSM-coated interconnects after oxidation was much thinner than that of bare interconnects. As the conductivity of LSM was higher than that of bare steel, the coated steel was evaluated to have a lower high-temperature ASR, which coincided with the results demonstrated in Figure 5.

The coating on metallic interconnects acts as anti-oxidation layer for high temperature exposure, and can ensure the stable performance of interconnects during operation [24]. Additionally, if the outermost layer of coated interconnects directly comes in contact with the cell electrode for planar SOFC stacks, the contact can be improved greatly by the two

similar properties of the material [25]. By contrast, when the oxide scale on the bare interconnect surface comes in direct contact with the cell electrode, the contact characteristics are entirely different from those of the contact method mentioned above. Moreover, the oxide scale can increase contact resistance, as reported in Refs. [26–28]. Therefore, the ASR of cathode sandwich structure 2 was smaller than that of cathode sandwich structure 3. LSM coating on interconnects can reduce the ASR of the cathode sandwich structure due to the improvement of contact between cathodes and interconnects.

As the contact resistance between the cathodes and interconnects was the main source of stack resistance, optimizing the cathode contact method was crucial. Real surfaces are not flat, and the contacts are made of numerous contact points. These points, termed a-spots, provide the only conducting paths for the transfer of electrical current [29]. In general, contact resistance can be expressed as a sum of the constriction resistance contribution and scale resistance contribution [30–33]. According to Holm's [29] and Greenwood's [34] theories, the constriction resistance between two materials with resistivities of ρ_1 and ρ_2, can be given as

$$R_c = (\rho_1 + \rho_2)\left(\frac{1}{4na} + \frac{1}{4a}\right) \tag{2}$$

where ρ_1 and ρ_2 are the resistivity values of the metals in contact, a is the radius of the a-spots, n is the number of circular a-spots, and a can be defined as the Holm radius:

$$a^{-1} = \frac{3\pi}{16n^2} \tag{3}$$

However, the surfaces are not clean, and the passage of electric current may be affected by thin oxide or other low-conductivity films. Consequently, the total contact resistance of a joint is the sum of the constriction resistance (R_s) and the film resistance (R_f)

$$R_c = R_s + R_f$$
$$R_f = \frac{\sigma \times l}{s} \tag{4}$$

where σ is the resistance of the film, l is the thickness of the film, and s is the contact area [28].
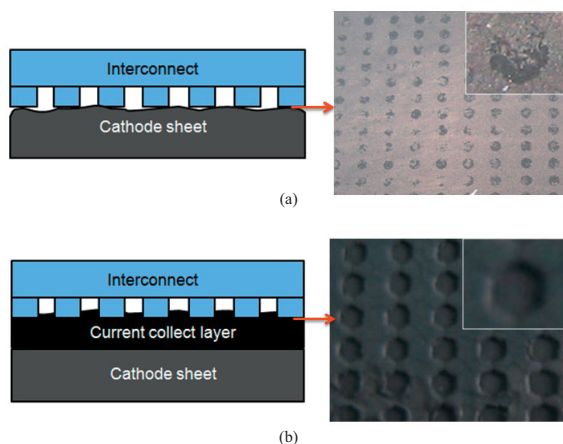

Fig. 11 Schematic demonstration of (a) surface contact and (b) immersed contact between the interconnect and the cathode.

When the interconnect and the cathode sheet were brought into direct contact, as demonstrated in Figure 11a, this contact method will only touch over a little fraction of the cross-sectional area due to the inherent roughness of both components. The contact resistance could be given as

$$R_c^1 = (\rho_{IT} + \rho_{LSM-YSZ})\left(\frac{1}{4n_1 a} + \frac{1}{4a_1}\right) \tag{5}$$

where ρ_{IT} and $\rho_{LSM-YSZ}$ are resistivities of the interconnect and cathode sheet, respectively; n_1 is the number of circular a-spots; and a_1 is the Holm radius.

However, when a cathode current collecting layer was used, the contact resistance could be demonstrated as

$$R_c^2 = (\rho_{IT} + \rho_{LSM})\left(\frac{1}{4n_2 a} + \frac{1}{4a_2}\right) + R_f \tag{6}$$

where ρ_{LSM} is the resistivity of the current collecting layer.

The LSM–YSZ cathode sheet used in this work was tested to be 10 S cm^{-1} by 4-probe method. And the conductivity of porous LSM material, Ni–YSZ anode sheet at 800 °C was around 20 S cm^{-1} [35], 1,200 S cm^{-1} [36], respectively. Thus, according to Eq. (4), the R_f of porous 250 μm thick LSM current collecting layer and 450 μm thick LSM–YSZ cathode sheet was calculated to be 1.25 and 4.5 mΩ cm^2, which shared only 1 and 3.6% of the maximum resistance between the cathode sheet and interconnect. Thus, the scale resistance of the current collecting layer was negligible compared with the total contact resistance. The contact resistance could then be simplified as

$$R_c^2 = (\rho_{IT} + \rho_{LSM})\left(\frac{1}{4n_2 a} + \frac{1}{4a_2}\right) \tag{7}$$

The application of a cathode current collecting layer made the metal interconnect tips immerge into the soft structure of LSM easily, as demonstrated in Figure 11. The immerged tips resulted in more contact area and the increased contact area resulted in more contact points, i.e. n_2–n_1. . . . Meanwhile, the Holm radius had an inverse relationship with the number of contact points, as shown in Eq. (3). However, the radius of a-spots, "a", did not change in this research as it was only dependent on the load [21]. In consequence, R_c^2 was smaller than R_c^1, as n_2–n_1, a_2–a_1, and ρ_{LSM}–$\rho_{LSM-YSZ}$. Therefore, using a cathode current collecting layer on the cathode sheet were helpful to improve contact between cathode components and reduce contact resistance.

Figure 12a shows the degradation curve of repeating unit (containing one piece of unit cell and one piece of interconnect) inside stack under thermal cycling. The original operation voltages of the repeating unit 1, 2, and 3 at 800 °C were 0.8, 0.88, and 0.9 V, respectively, under the condition of 0.1 A cm^{-2} discharging current and H$_2$/Air = 5/15 sccm cm^{-2} gas flow rate. The degradation rates of repeating unit 1, 2, and 3 were 19.1, 6.7, and 10.2% for five thermal cycles (i.e. a degradation of 3.82, 1.34, and 2.04% per cycle), respectively. The OCVs of the repeating units remained almost 1.2 V under the thermal cycling condition, indicating good sealing performance in the stack during
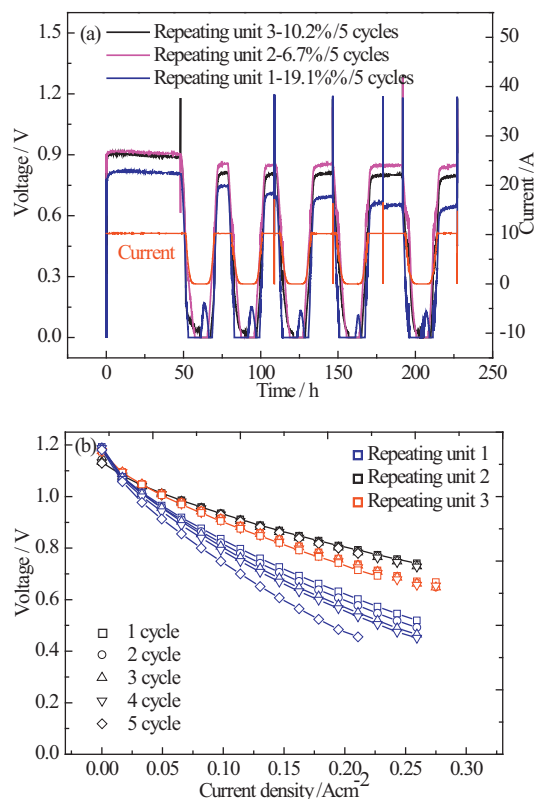
Fig. 13 ASR changing of different repeating units in stack during thermal cycling.

Fig. 12 (a) Degradation and (b) I–V curves of different stack repeating units inside stack under thermal cycles.

operation. Accordingly, it could be inferred that the degradation of repeating unit is independent of stack sealing. According to our previous research [22], it could also be inferred that the degradation of repeating unit was mainly dependent on the contact between interconnects and electrodes. Figure 12b shows the I–V curves of repeating units after every cycle. By fitting the I–V curve, the ASR values of repeating units was obtained, and demonstrated in **Figure 13**. The ASRs of repeating units 1 and 2 inside the stack have a similar changing trend to that of the corresponding cathode sandwich, while the ASR changing of repeating unit 3 was different from the sandwich result perhaps due to increasing ASR of cell itself. The ASR values of optimized contact with LSM coated interconnect and LSM cathode current collecting layer were about four times larger than that of corresponding cathode sandwich, which was perhaps due to that the ASR of unit cell used in the stack was much larger than that of cathode sheet. It was obvious that the contact between coated interconnect and current collecting layer on cell cathode side has the lowest and most stable ASR value for planar SOFCs during both isothermal and cycling conditions. Therefore, the coating on interconnect and current collecting layer on electrode can reduce the ASR of stack repeating unit, and thus improve the stack performance.
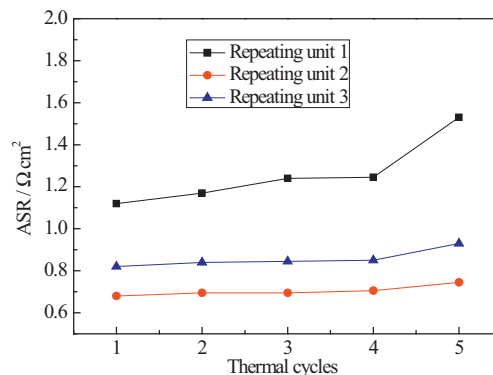
4 Conclusion

The ASR of SUS430/Ni–YSZ/SUS430 anode sandwich with NiO current collecting layer on Ni–YSZ sheet remained about 0.004 Ω cm^2 under isothermal operation, and increased to 0.006 Ω cm^2 after one thermal cycle, and then remained stable during thermal cycling. While the ASR of SUS430/Ni–YSZ/SUS430 anode sandwich without NiO current collecting layer remained 0.003 Ω cm^2 under isothermal operation, and increased rapidly to 0.015 Ω cm^2 after one thermal cycle and then continued to increase with thermal cycles. The ASR of SUS430/LSM–YSZ/SUS430 cathode sandwich with LSM coated interconnect and LSM current collecting layer on LSM–YSZ sheet remained about 0.1 Ω cm^2 during isothermal oxidation, and increased slightly to 0.16 Ω cm^2 after five thermal cycles. The ASR of SUS430/LSM–YSZ/SUS430 cathode sandwich assembled by bare interconnect and LSM current collecting layer on LSM–YSZ sheet increased rapidly from 0.1 to 0.9 Ω cm^2 within 72 hours' isothermal oxidation, and then remained about 1.0 Ω cm^2 before thermal cycling. After one cycle, the ASR increased to about 1.3 Ω cm^2, and then decreased slowly with thermal cycles. After six thermal cycles, the ASR reached 1.0 Ω cm^2. The largest ASR of contact between interconnects and electrodes existed in SUS430/LSM–YSZ/SUS430 cathode sandwich with bare inteconnect and LSM–YSZ sheet without current collecting layer. The ASR increased sharply from 0.9 to 1.2 Ω cm^2 within 25 hours' isothermal oxidation, and then remained about 1.2 O cm^2 during isothermal operation before thermal cycling. After one thermal cycle, the ASR increased enormously to 3.9 Ω cm^2, and then remained increasing trends with thermal cycles.

A three-cell stack was assembled by three interfacial contact methods between interconnects and electrodes. The first one is the contact between uncoated interconnect and cathode without current collecting layer. The second is the contact between uncoated interconnect and cathode with current collecting layer. The last is the contact between coated interconnect and cathode with current collecting layer. The degradation rate of corresponding repeating unit reached 3.82, 2.04, and 1.34% per cycle with ASR increasing rates of 7.3, 2.7, and 1.9% per cycle, respectively, indicating that the application of

LSM protective coating on interconnect and LSM current collecting layer on cell cathode side could reduce the contact resistance between interconnects and their adjacent component, and then improve the stack durability during isothermal and thermal cycling conditions.

Acknowledgements

References

[1] T. L. Wen, D. Wang, H. Y. Tu, M. Chen, Z. Lu, Z. Zhang, H. Nie, W. Huang, *Solid State Ionics* **2002**, *399*, 152.

[2] J. W. Fergus, *Mater. Sci. Eng. A* **2005**, *397*, 271.

[3] W. Z. Zhu, S. C. Deevi, *Mater. Res. Bull.* **2003**, *38*, 957.

[4] J. W. Wu, X. B. Liu, *J. Mater. Sci. Technol.* **2010**, *26*, 293.

[5] J. Pu, J. Li, B. Hua, G. Xie, *J. Power Sources* **2006**, *158*, 354.

[6] B. Hua, J. Pu , F. S. Lu, J. F. Zhang, B. Chi, J. li, *J. Power Sources* **2010**, *195*, 2782.

[7] T. Brylewski, M. Nanko, T. Maruyama, K. Przybylski, *Solid State Ionics* **2001**, *143*, 131.

[8] L. Cooper, S. Benhaddad, A. Wood, D. G. Ivey, *J. Power Sources* **2008**, *184*, 220.

[9] J. Froitzheim, G. H. Meier, L. Niewolak, P. J. Ennis, H. Hattendorf, L. Singheiser, W. J. Quadakkers, *J. Power Sources* **2009**, *178*, 163.

[10] M. F. Han, S. P. Peng, Z. L. Wang, Z. B. Yang, X. Chen, *J. Power Sources* **2007**, *164*, 278.

[11] S. P. Jiang, *Int. J. Hydrogen Energy* **2012**, *39*, 449.

[12] B. M. An, W. Zhou, Y. M. Guo, R. Ran, Z. P. Shao, *Int. J. Hydrogen Energy* **2010**, *35*, 5601.

[13] J. I. Gazzarri, O. Kesler, *J. Power Sources* **2008**, *176*, 138.

[14] Z. G. Yang, G. G. Xia, P. Singh, J. W. Stevenson, *J. Power Sources* **2006**, *155*, 246.

[15] S. P. Jiang, J. G. Love, L. Apateanu, *Solid State Ionics* **2003**, *160*, 15.

[16] T. Dey, D. Singdeo, M. Bose, R. N. Basu, P. C. Ghosh, *J. Power Sources* **2013**, *233*, 290.

[17] B. Morel, M. Reytier, B. Oresic, *The 9th European Solid Oxide Fuel Cell Forum*, Lucerne, Switzerland, **2010**, pp. 12.

[18] C. Magnière, S. Di Iorio, B. Morel, *ECS Trans.* **2011**, *35*, 1841.

[19] J. X. Wang, J. Shao, Y. K. Tao, W. G. Wang, *J. Power Sources* **2009**, *186*, 344.

[20] S. S. Pyoa, S. B. Lee, T. H. Lim, R. H. Song, D. R. Shin, S. H. Hyun, Y. S. Yoo, *Int. J. Hydrogen Energy* **2011**, *36*, 1868

[21] S. Koch, P. V. Hendriksen, *Solid State Ionics* **2004**, *168*, 1.

[22] W. B. Guan, L. Jin, X. Ma, W. G. Wang, *Fuel Cells* **2012**, *12*, 1085.

[23] L. Jin, W. B. Guan, J. Q. Niu, X. Ma, W. G. Wang, *J. Power Sources* **2013**, http://dx.doi.org/10.1016/j.jpowsour.2013.04.027.

[24] N. Shaigan, W. Qu, D. G. Ivey, W. X. Chen, *J. Power Sources* **2010**, *195*, 1529.

[25] M. Braunovic, Valery V. Konchits, Nikolai K. Myshkin, *Electrical Contacts – Fundamentals, Applications and Technology*, CRC press, Boca Raton, FL, USA, **2006**.

[26] H. Ebrahimifar, M. Zandrahimi, *Ionics* **2012**, *18*, 615.

[27] S. Megel, E. Girdauskaite, V. Sauchuk, M. Kusnezoff, A. Michaelis, *J. Power Sources* **2011**, *196*, 7136.

[28] W. A. Meulenbers, S. Uhlenbruck, E. Wessel, H. P. Buchkremer, D. Stover, *J. Mater. Sci.* **2003**, *38*, 507.

[29] R. Holm, *Electrical Contacts*, Springer, New York **1979**.

[30] N. Q. Minh, T. Takahashi, *Science and Technology of Ceramic Fuel Cells*, Elsevier, Amsterdam, The Netherlands, **1995**.

[31] C. Bagger, M. Juhl, P. V. Hendriksen, P. H. Larsen, M. Mogensen, *Proc. 2nd European Solid Oxide Fuel Cell Forum 1, European Solid Oxide Fuel Cell Forum*, Oberrohrdorf, Switzerland, **1996**, pp. 175.

[32] J. Fleig, J. Maier, *Proc.5th International Symposium on Solid Oxide Fuel Cells*, (*SOFC-V*), Pennington, NJ, USA, **1997**, pp. 1374.

[33] C. Bagger, S. Linderoth, M. Mogensen, P. V. Hendriksen, B. Kindl, S. Larsen, P. H. Larsen, F. W. Poulsen, N. Bonanos, M. J. Jørgensen, *Proc. 6th International Symposium on Solid Oxide FuelCells* (*SOFC-VI*), Pennington, NJ, USA, **1999**, pp. 28.

[34] J. A. Greenwood, *Br. J. Appl. Phys.* **1966**, *17*, 1621.

[35] L. Grahl-Madsen, IRD A/S, personal correspondence, **2000**.

[36] C. R. He, W. G. Wang, *Fuel Cells* **2009**, *9*, 630.